ACS OMEGA

Open Access

http://pubs.acs.org/journal/acsodf

Article

Comprehensive Proteomic Profiling of Aqueous Humor in Idiopathic Uveitis and Vogt−Koyanagi−Harada Syndrome

Lingzi Wu,[▽] Jinying An,[▽] Xueru Li,[▽] Qingqin Tao, Zheng Liu, Kai Zhang, Lei Zhou, and Xiaomin Zhang*

Cite This: *ACS Omega* 2024, 9, 18643−18653

Read Online

ACCESS | Metrics & More | Article Recommendations | Supporting Information

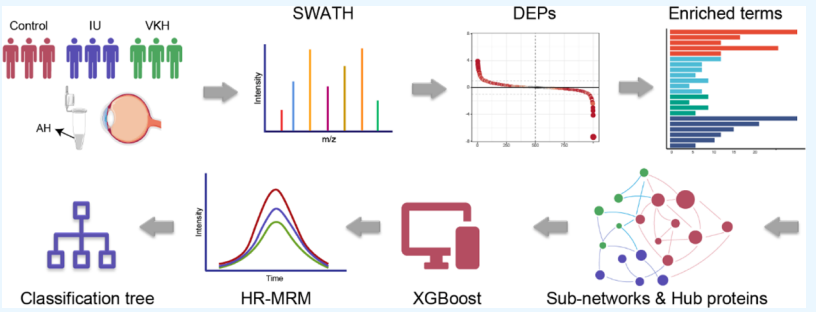

ABSTRACT: Idiopathic uveitis (IU) and Vogt−Koyanagi−Harada (VKH) syndrome are common types of uveitis. However, the exact pathological mechanisms of IU and VKH remain unclear. Proteomic analysis of aqueous humor (AH), the most easily accessible intraocular fluid and a key site of uveitis development, may reveal potential biomarkers and elucidate uveitis pathogenesis. In this study, 44 AH samples, including 12 IU cases, 16 VKH cases, and 16 controls, were subjected to label-free quantitative proteomic analysis. We identified 557 proteins from a comprehensive spectral library of 634 proteins across all samples. The AH proteomic profiles of the IU and VKH groups were different from those of the control group. Differential analysis revealed a shared pattern of extracellular matrix disruption and downregulation of retinal cellular proteins in the IU and VKH groups. Enrichment analysis revealed a protein composition indicative of inflammation in the AH of the IU and VKH groups but not in that of the control group. In the IU and VKH groups, innate immunity played an important role, as indicated by complement cascade activation and overexpression of innate immune cell markers. Extreme gradient boosting (XGBoost), an efficient and robust machine learning algorithm, was subsequently used to screen potential biomarkers for classifying the IU, VKH, and control groups. Transferrin and complement factor B were deemed the most important and represent a promising biomarker panel. These proteins were validated by high-resolution multiple reaction monitoring (HR-MRM) in an independent validation cohort. A classification decision tree was subsequently built for the diagnosis. Our findings further the understanding of the underlying molecular mechanisms in IU and VKH and facilitate the development of potential therapeutic and diagnostic strategies.

1. INTRODUCTION

Uveitis is a sight-threatening disease characterized by intraocular inflammation of the uveal tract and adjacent structures and accounts for 5−10% of visual impairment worldwide.[1] According to the International Uveitis Study Group, the etiological classification distinguishes three types of uveitis: infectious uveitis, noninfectious uveitis (NIU), and masquerade.[2] Among clinically diagnosed NIU, idiopathic uveitis (IU) predominates, accounting for 24−55% of cases.[3] Vogt−Koyanagi−Harada (VKH) syndrome is another common NIU type and is a major vision-threatening disease in Asian populations.[4,5] The pathogenesis of both IU and VKH remains unclear. Additionally, IU and VKH lack specific laboratory findings, thus necessitating the identification of diagnostic biomarkers.

Aqueous humor (AH) is a transparent fluid that bathes the anterior and posterior chambers of the eye, provides nutrients to the ocular tissues, and is essential to the overall functioning of the eye. Furthermore, AH is the direct metabolic region of ocular tissues and one of the most frequently used fluid ocular matrices for human biomarker evaluation. The onset and progression of numerous ocular diseases, including posterior segment disease,[6,7] may influence AH components. Current evidence suggests the existence of a significant physiological

Received: February 18, 2024
Revised: March 29, 2024
Accepted: April 3, 2024
Published: April 15, 2024

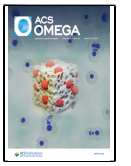

flow of AH through the vitreous humor and across the retinal pigment epithelium, which exits the eye via the choriocapillaris and vortex veins.[8] For humans, in particular, this posteriorly directed flow is approximately equal to the anteriorly directed flow. A recently published paper in *CELL* revealed that 87.0% (5172) of vitreous proteins could be identified in AH demonstrating a substantial protein exchange between both fluid-filled compartments.[9] In addition, the authors found that cell-specific intracellular proteins from the retina could be detected in AH and that proteins from photoreceptors and ciliary body cell origins were also strongly enriched in AH. Therefore, substance exchange among the AH, vitreous humor, and retina makes proteomic studies of AH valuable for understanding posterior segment diseases of the eye, including panuveitis. Given the low invasiveness, renewability, and intraocular microenvironmental origin of AH, we can identify AH-derived biomarkers for VKH and IU and explore intraocular molecular characteristics in affected eyes by analyzing the AH proteome.

In this study, we performed proteomic analysis of AH from patients with IU and VKH and investigated the underlying pathogenic mechanism by using comprehensive bioinformatic analysis. In addition, we identified a potential diagnostic biomarker panel and established a classification decision tree for differentiating IU and VKH, and control groups using a machine learning method.

2. METHODS

2.1. Subjects and Sample Collection. Forty-four participants, including patients diagnosed with IU (n = 12), VKH (n = 16), and cataract, which comprised the control group (n = 16), were recruited for sequential window acquisition of all theoretical fragment ions (SWATH) analysis. Additionally, 24 participants, diagnosed with IU (n = 8), VKH (n = 8), and cataract (n = 8) were recruited for high-resolution multiple reaction monitoring (HR-MRM) analysis. For patients with IU and VKH manifesting as panuveitis, AH samples were obtained during cataract surgery when ocular inflammation was inactive and the anterior chamber cell grade was 0. The control group was composed of patients with age-related cataracts without any other ocular diseases. All procedures complied with the Declaration of Helsinki, and ethical approval was obtained from the Ethics Committee of Tianjin Medical University Eye Hospital, Tianjin, China (approval number. 2020KY(L)-56). All of the participants provided written informed consent.

2.2. Sample Preparation for Mass Spectrometry Analysis. Approximately 50 μL of AH samples was resuspended in 200 μL of 8 M urea lysis buffer (8 M urea, 1 mM NaF, 1 mM Na_3VO_4, 50 mM NH_4HCO_3, and 1× complete protease inhibitor mixture), and the protein content was determined using a bicinchoninic acid assay (Solarbio, China). Equal amounts of the total protein obtained from each sample were reduced or alkylated with dithiothreitol or iodoacetamide, respectively. Subsequently, the samples were loaded onto a Vivacon 500 centrifugal concentrator (Sartorius, Germany) and trypsinized (Promega) at a 50:1 protein-to-enzyme ratio for 12−16 h at 37 °C. The digested peptide fragments were eluted with 50 mM NH_4HCO_3 (>99.5%, Sigma-Aldrich), after which the reaction was quenched with 1% (v/v) formic acid (FA, 98−100%, Merck, Germany). Peptides were dried using an integrated SpeedVac (Thermo Scientific) and then resuspended in 1‰ (v/v) FA.

2.3. Spectral Library Construction. A reference spectral library was constructed for the SWATH acquisition. Small amounts of each sample were collected and pooled to construct a cohort-specific spectral library. The pooled sample was fractionated into nine fractions using a high-pH reversed-phase microcolumn (Durashell C18, DC930010-L, Agela, China). The obtained fractions were processed as described in Section 2.2 and analyzed by liquid chromatography−tandem mass spectrometry (LC−MS/MS) using a nano-LC 415 (Eksigent Technologies) and a triple time-of-flight (TOF) 6600 mass spectrometer (AB Sciex) in information-dependent acquisition (IDA) mode. A micro ion source was used for this analysis. The peptide fragments were loaded onto a custom-made trap column (10 × 0.3 mm, Durashell C18 5 μm, 120 Å) and separated using a custom-made analytical column (150 × 0.3 mm, Durashell C18 3 μm, 120 Å) at flow rates of 10 and 5 μL/min, respectively. The peptides were resolved over a 60 min nano-LC gradient (linear gradient from 5 to 80% LC buffer B [0.1% FA and 2% water in acetonitrile] over 55 min and then to 5% buffer B over 5 min). For data acquisition in IDA mode, TOF−MS spectra were recorded across a 300−1500 m/z range with an accumulation time of 0.25 s. Ion selection criteria included a charge state between +2 and +5, a mass tolerance of 50 ppm, and an intensity above 150 cps. A maximum number of 60 candidate ions were monitored per cycle; the time of excluding former target ions was always 15 s after one occurrence, and a dynamic fragmentation pattern was chosen. Tandem MS across a 100−1500 m/z range was performed using dynamic fragmentation with various collision energies (CEs) and a high-sensitivity scanning mode with an accumulation time of 0.035 s.

2.4. Quantitative Proteomic Data Acquisition. Forty-four independent samples were analyzed using SWATH-MS. For each sample, 1 μg of peptide was injected. For SWATH experiments, the accumulation time of TOF−MS was 0.25 s, and the high-sensitivity scanning mode was selected for MS/MS. Furthermore, based on the SWATH variable window calculator v1.1, 94 variable windows were developed. An accumulation time of 34 ms was used for each window. The scanning mass range was 100−1500 Da. Other parameters were the same as those used in the IDA mode for spectral library construction.

2.5. Validation by HR-MRM. Twenty-four samples were analyzed using HR-MRM. For each sample, 3 μg of peptide was injected. HR-MRM was performed in standard acquisition mode with 70 variable windows and a 46 ms accumulation time per window. TOF−MS scans of individual candidate peptides were set to their m/z values, followed by MS/MS product ion scans of 100−1500 Da. CEs were calculated as CEs = (m/z × 0.049) − 4 for +2 charge peptides and CEs = (m/z × 0.048) − 3 for +3 charge peptides. The CEs equation was based on a previously published study[10] and optimized to fit our instrument. Other parameters were the same as those used in IDA mode for spectral library construction.

2.6. Data Processing. Raw data from IDA mode were analyzed using ProteinPilot software (v.5.0.1; AB Sciex) with reference to the UniProt human database (released 2020_03), which contains 20,368 annotated proteins with a false discovery rate (FDR) < 1%. SWATH-MS results were processed using the SWATH Acquisition Micro application (v.2.0) in PeakView (v.2.2; AB Sciex) software, with reference to the spectral library. During processing, we selected an extraction window of 12 min and the following conditions: six

https://doi.org/10.1021/acsomega.3c10257
ACS Omega 2024, 9, 18643−18653

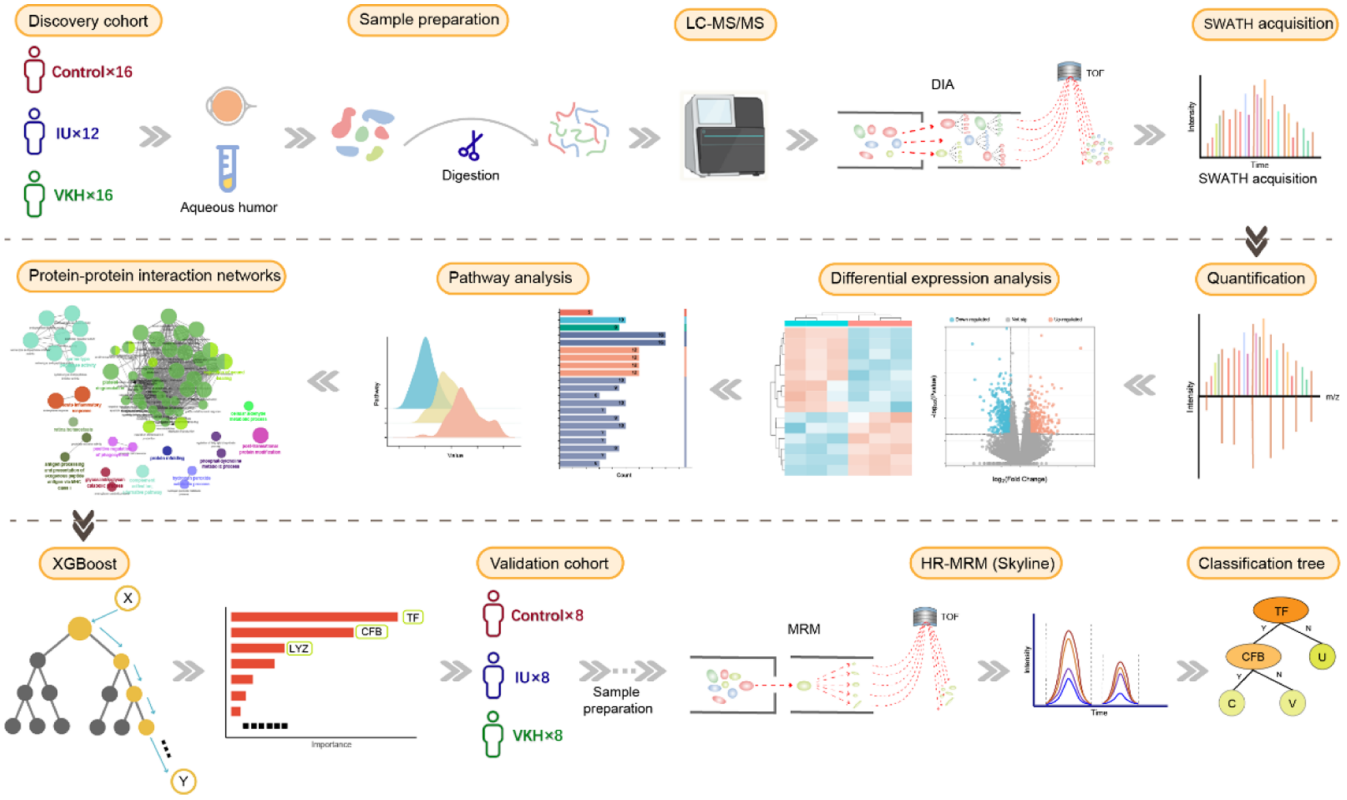

Figure 1. Summarized workflow of the aqueous humor proteomic analysis. Aqueous humor samples (n = 44) were subjected to LC−MS/MS analysis in the SWATH method based on an established cohort-specific spectral library; obtained data were analyzed for differential expression analysis, pathway analysis, and protein−protein interaction analysis; Biomarker candidates were identified using the XGBoost algorithm and validated by HR-MRM; Classification decision tree was built.

peptides and six transitions, excluding shared and modified peptides; an XIC width of 50 ppm; peptide confidence >99%; and FDR < 1%. The peak areas were exported as quantitative values. Data obtained from HR-MRM was imported into Skyline software (v.20.1.0.155; http://proteome.gs.washington.edu/software/skyline/). Peptide retention time was calibrated according to the spectral library, and the peptide quantitative values were then exported. Three peptides from each protein were chosen for quantification, and the final protein quantitative values were determined by the sum of the peptides. The peptide sequences were as follows: TF, SAGWNIPIGLLYCDLPEPR/MYLGYEYVTAIR/DYELLCLDGTR; CFB, LEDSVTYHCSR/DLLYIGK/DAQYAPGYDK; LYZ, WESGYNTR/STDYGIFQINSR/QYVQGCGV.

The quantitative data were log 2-transformed and median-normalized. Differential analysis was performed using the "t test" function in the "stats" R package. Proteins with a fold-change (FC) > 1.5 or < −1.5, and p-values <0.05 were considered differentially expressed proteins (DEPs).

2.7. Bioinformatics Analysis. Principal component analysis (PCA) score plots and box plots and complexity parameter (cp) plots were obtained using the "factoextra", "ggpubr" R packages, and "plotcp" R function. Abundance scatter plots, volcano plots, bar graphs, ridge-line plots, and matrix heatmap were constructed using the online biomedical visualization software Hiplot (https://hiplot.com.cn), bioinformatics (https://bioinformatics.com.cn), and Bioladder (https://www.bioladder.cn/). Heatmaps were visualized by using the "pheatmap" R package. The resultant plots were adjusted using Adobe Illustrator (Adobe). Gene ontology (GO) enrichment analyses were performed using Metascape online analysis software (http://metascape.org).[11] Gene set enrichment analysis (GSEA) and gene set variation analysis (GSVA) were performed using the "clusterProfiler" and "GSVA" R packages, respectively, and utilized the molecular signature database (MSigDB, c5.go.bp.v2023.1.Hs.entrez.gmt/msigdb.v2023.1.Hs.symbols.gmt). Pathway RespOnsive GENes for activity inference (PROGENy) was performed using the "progeny" R package. Protein−protein interaction (PPI) networks were generated using STRING (https://cn.string-db.org/). Subworks and hub proteins were identified using the molecular complex detection (MCODE) and Cytohubba plugins, respectively, for Cytoscape (version 3.9.0), implementing the maximum clique centrality (MCC) algorithm for CytoHubba.

2.8. Machine Learning. The data sets were randomly split in a 7:3 ratio to generate the training and testing data sets. Extreme gradient boosting (XGBoost) was used to screen potential biomarkers by using the "xgboost" R package. Fivefold cross-validation was performed using the "xgb.cv" R function. The xgb.importance" and "pROC," R packages were used to generate protein importance rankings and construct receiver operating characteristic (ROC) curves, respectively. In addition, a classification decision tree was built and plotted by using the "rpart" and "rpart.plot" R package, respectively.

2.9. Statistical Analyses. Statistical analyses were performed using SPSS software (v.24.0; IBM Corp). Data are presented as mean ± standard deviation. For normal data with even variance, Student's t tests were used; otherwise,

https://doi.org/10.1021/acsomega.3c10257
ACS Omega 2024, 9, 18643−18653

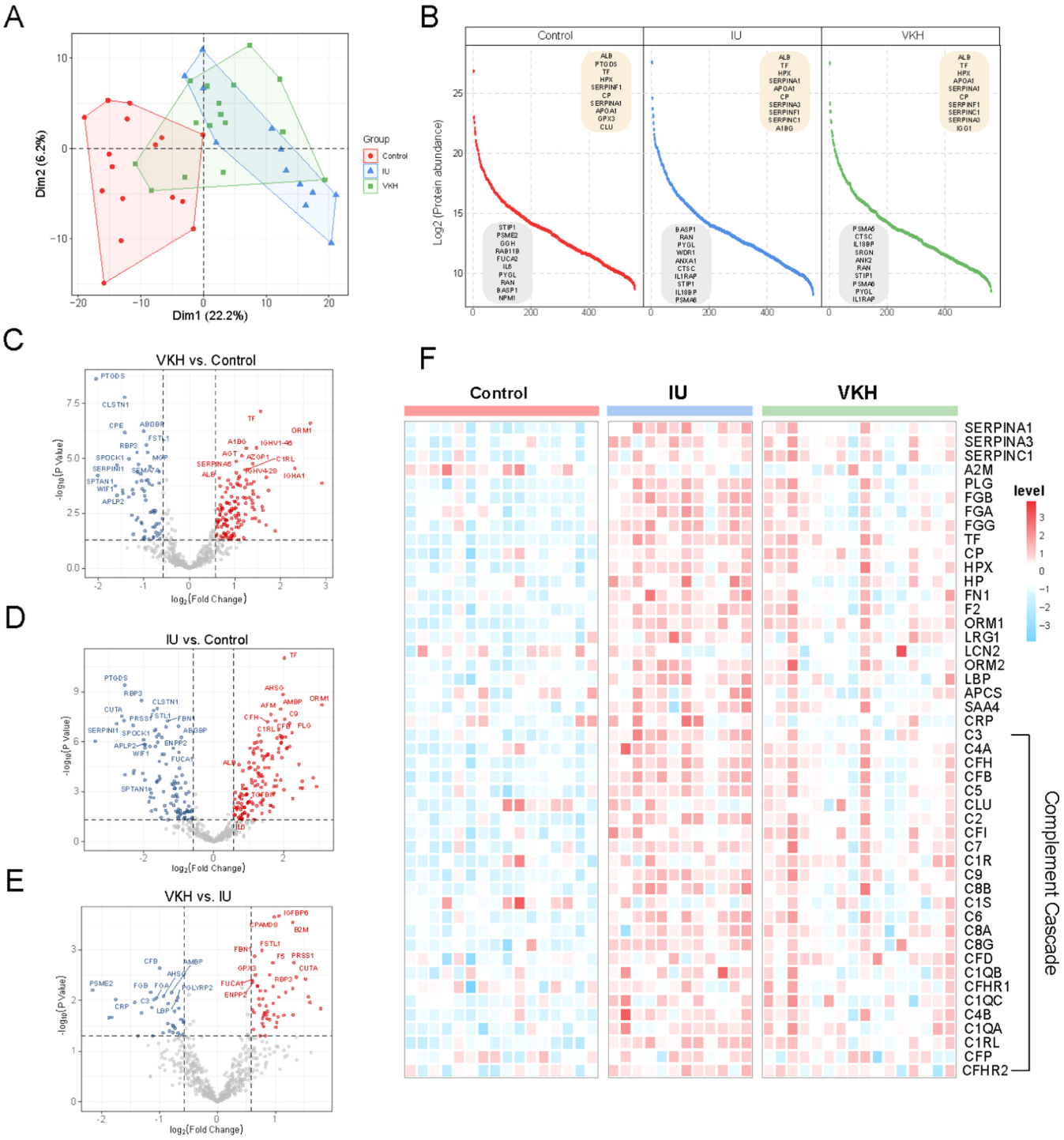

Figure 2. Characterization of the aqueous humor proteome in VKH, IU, and control groups. (A) Score plots of principal component analysis. (B) Ranked scatter plot showing the relative abundance of proteins identified in the aqueous humor with the top and bottom 10 proteins listed on yellow and gray backgrounds, respectively. (C) Volcano plot of differentially expressed proteins (DEPs) of VKH and control groups. Red, upregulated; blue, downregulated. (D) Volcano plot of DEPs of the IU and control groups. Red, upregulated; blue, downregulated. (E) Volcano plot of DEPs of the VKH and IU groups. Red, upregulated; blue, downregulated. (F) Heatmap showing the expression values of all of the identified acute phase proteins (APPs) in this study. Red, high expression; blue, low expression.

Mann−Whitney rank tests were used. Gender comparisons between the two groups were performed by using the chi-square test.

3. RESULTS

3.1. Workflow of Aqueous Humor Proteomic Analysis. The workflow of this study is displayed in Figure 1. Forty-four AH samples from patients with IU, VKH, and controls were used for SWATH analysis. Demographic parameters of the patients are summarized in Table S1. The obtained quantitative proteomic data were subjected to differential expression, enrichment, and PPI network analyses. Potential biomarker candidates were identified using the XGBoost machine learning algorithm and validated in an

https://doi.org/10.1021/acsomega.3c10257
ACS Omega 2024, 9, 18643−18653

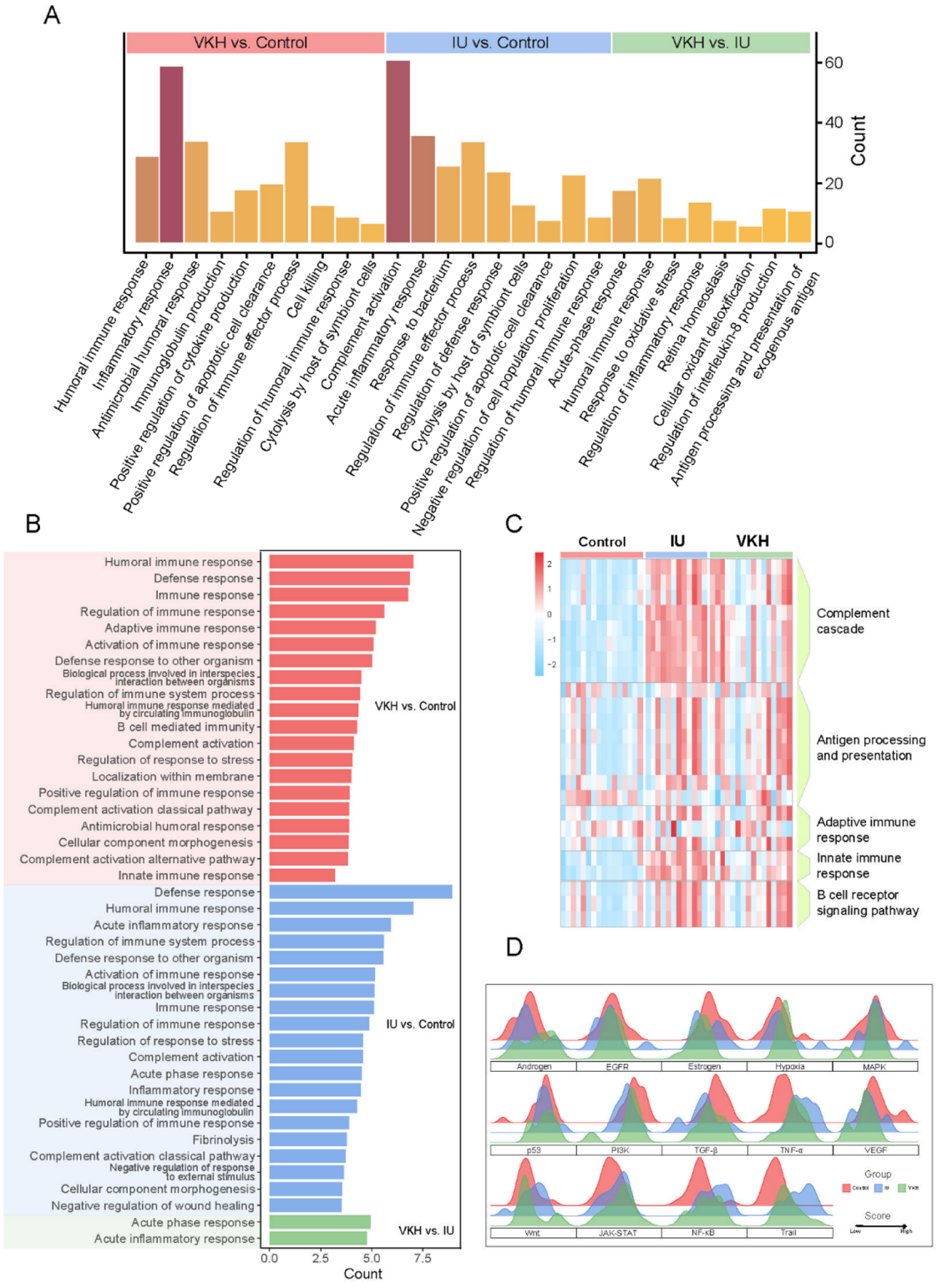

Figure 3. Enrichment analysis of differentially expressed proteins. (A) Bar graph showing the results of biological process GO analysis of DEPs of any two groups. (B) Bar graph showing the results of GSEA between any two groups. (C) Heatmap showing the results of GSVA in VKH, IU, and the control group. (D) Ridge-line plots showing the results of PROGENy analysis in VKH, IU, and the control group.

independent cohort using HR-MRM. Finally, a classification decision tree was built. Demographic parameters of the subjects in the validation cohort are listed in Table S1.

3.2. Differential Proteomic Profiling among IU, VKH, and Controls. *3.2.1. Characterization of the AH Proteome.* Based on IDA data, we constructed an AH-specific spectral library containing 634 proteins. Among these, we identified 557 proteins with an FDR < 1% across all samples using SWATH acquisition. Raw data were median-normalized. Box plots showing the data distribution before and after normalization are shown in Figure S1A,B, and the processed data are presented in Table S2. Pearson correlation coefficients

https://doi.org/10.1021/acsomega.3c10257
ACS Omega 2024, 9, 18643−18653

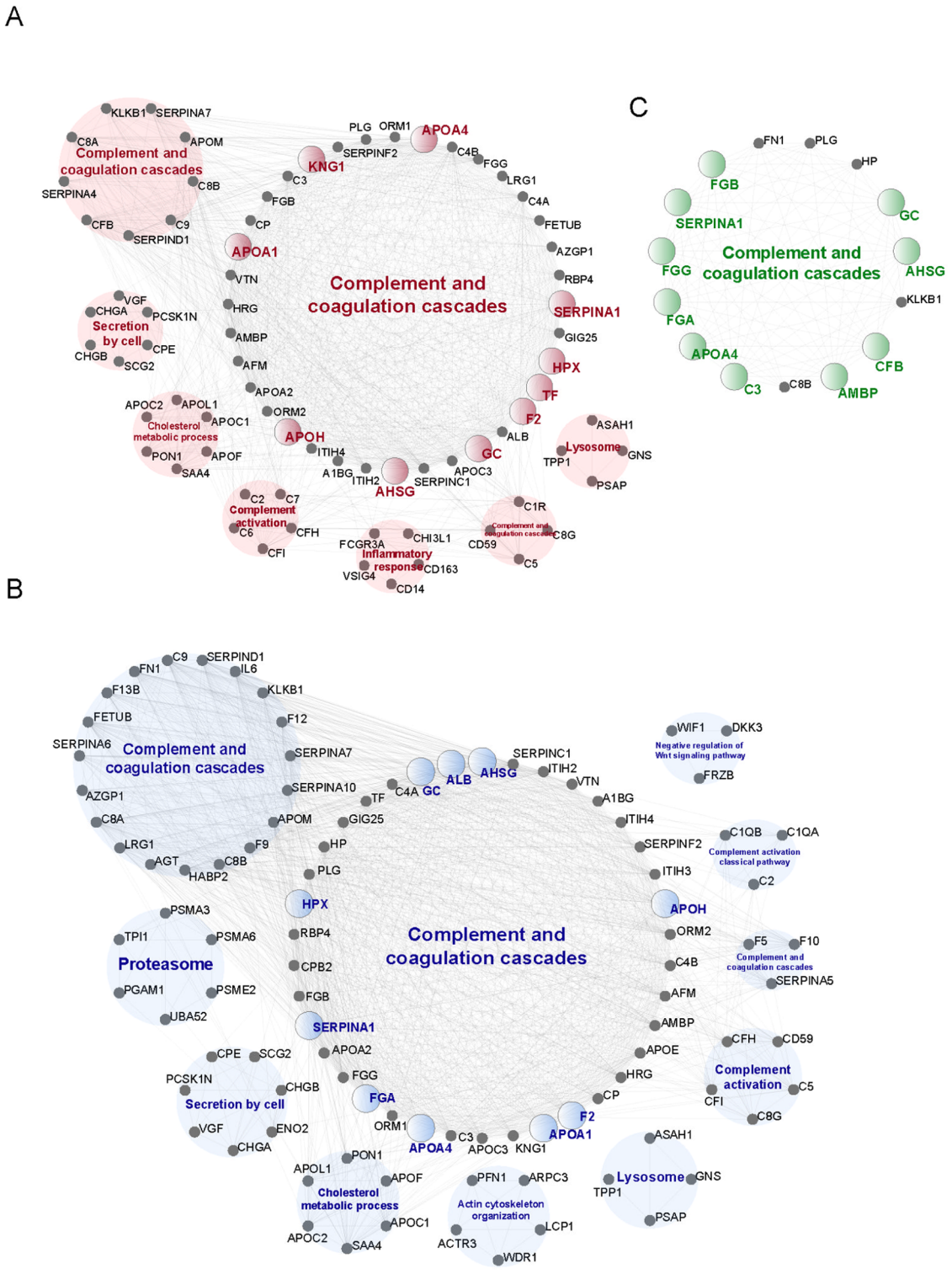

Figure 4. Identification of key subnetworks and hub proteins. (A) PPI network of DEPs of the VKH and control groups; the larger nodes indicate hub proteins. (B) PPI network of DEPs of the IU and control groups; the larger nodes indicate hub proteins. (C) PPI network of DEPs of the VKH and IU groups; the larger nodes indicate hub proteins.

between the samples were >0.72 (Figure S1C). Collectively, these results indicate the good quality of our proteomic data, which encourages further AH proteome analysis.

PCA based on the identified proteins revealed that the proteomic profiles of the VKH and IU groups differed from that of the control group, with higher intrasample variation in the VKH group than in the IU group (Figure 2A). Figure 2B displays the top 10 proteins with the highest and lowest mean abundances among the three groups. Across all groups, high protein abundance was seen for albumin (ALB), transferrin (TF), hemopexin (HPX), ceruloplasmin (CP), apolipoprotein A-I (APOA1), and members of the serpin family, whereas low protein abundance was seen for ras-related nuclear protein (RAN), glycogen phosphorylase (PYGL), stress-induced

https://doi.org/10.1021/acsomega.3c10257
ACS Omega 2024, 9, 18643−18653

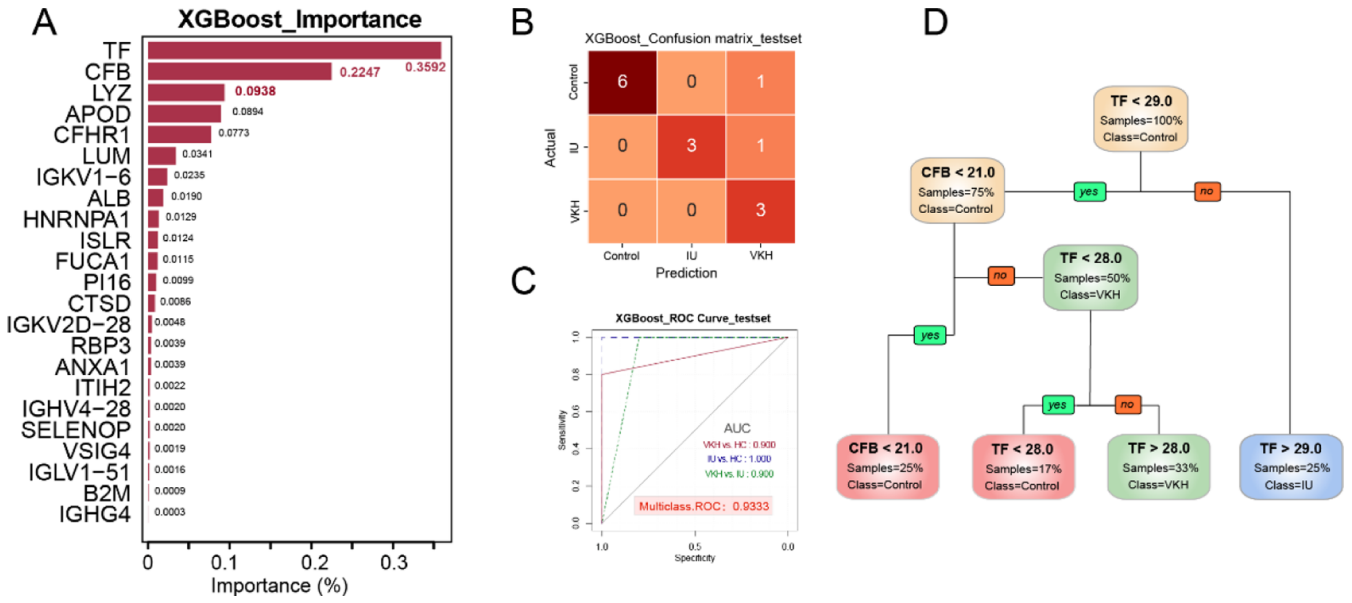

Figure 5. Generation and visualization of diagnostic classification models. (A) Bar graph showing protein importance scores in the XGBoost model. (B) Confusion matrix heatmap showing the classification results in the testing set of the XGBoost model. (C) ROC curve and AUC values of the XGBoost model for two-class and multiclass classification. (D) Classification decision tree showing the node information and threshold value.

phosphoprotein 1 (STIP1), proteasome subunits, and interleukins.

To compare the differential proteomic profiles of IU, VKH, and the control group, we performed differential analysis (Table S3) and identified 187 (VKH vs control), 241 (IU vs control), and 82 (VKH vs IU) DEPs with |FC| > 1.5 and $p < 0.05$. Compared with the control group, the VKH group had 126 upregulated and 61 downregulated DEPs, and the IU group had 138 upregulated and 103 downregulated DEPs. Compared with the IU group, the VKH group had 50 upregulated and 32 downregulated DEPs.

These DEPs are displayed in volcano plots (Figure 2C−E), with red dots representing upregulated proteins and blue dots representing downregulated proteins. Several inflammation-related proteins, such as TF, orosomucoid-1 (ORM1), and complement components, were overexpressed in the IU and VKH groups compared with the control group. Additionally, TGFB1 and IL6, with opposite inflammatory regulatory effects, were both upregulated in the IU group compared to those in the control group. Notably, several downregulated proteins in the IU and VKH groups overlapped, including prostaglandin-H2 D-isomerase (PTGDS), calsyntenin-1 (CLSTN1), follistatin-related protein 1 (FSTL1), and retinol-binding protein 3 (RBP3). Over 50% of the DEPs overlapped between the VKH and IU groups in either the up- or downregulated clusters (Figure S2A). To elucidate the function of the overlapping DEPs, we performed biological process GO analysis, which revealed that the overlapping downregulated DEPs are related to cell−cell adhesion, cell growth regulation, and eye morphogenesis, whereas the overlapping upregulated DEPs were mainly enriched in complement activation, acute inflammatory responses, and regulation of the humoral immune response (Figure S2B). Additionally, all of the identified acute phase proteins (APPs) exhibited greater expression in both the IU and VKH groups than in the control group (Figure 2F), and peaked in the IU group.

3.2.2. Enrichment Analysis of DEPs. To understand the biological processes occurring in AH under different disease states, we conducted biological process GO analysis (Figure 3A) and found that the DEPs of the VKH and control groups were enriched in "humoral immune response," "antimicrobial humoral response," "positive regulation of cytokine production", and "cell killing". For DEPs of the IU and control groups, "complement activation," "acute inflammatory response," "response to bacterium," and "regulation of defense response" were enriched. Additionally, DEPs of the VKH and IU groups exhibited significant enrichment of terms associated with "acute-phase response," "response to oxidative stress," and "regulation of interleukin-8 production."

To comprehensively understand the differential proteomic profiles of the IU, VKH, and control groups, GSEA, GSVA, and PROGENy analyses using all identified proteins were conducted. The results of the GSEA, performed based on protein expression FC-values generated from the differential analysis between any two groups, are listed in Figure 3B. Similar enrichment terms were found in the VKH and IU groups compared to the control group, including "humoral immune response," "defense response," and "complement activation," whereas "acute immune response" was specifically enriched in the IU group. Subsequent GSEA analysis comparing the VKH and IU groups also highlighted differential APPs expression (Figure 2F), which corresponds to the results of the biological process GO analysis of the DEPs (Figure 3A). GSVA is a nonparametric, unsupervised algorithm that calculates enrichment scores for specific gene sets in each sample without group differentiation. Figure 3C shows the GSVA scores for 44 samples in immune-related biological processes and pathways and indicates that "complement cascade," "antigen processing and presentation," "adaptive immune response," "innate immune response", and "B cell receptor signaling pathway" scored higher for both IU and VKH than for the control, implying an upregulated state. PROGENy was used to infer the relative pathway activity from gene expression under a wide range of conditions using publicly available perturbation experiment data.[12] Figure 3D shows the relative activity states of 14 pathways inferred using

https://doi.org/10.1021/acsomega.3c10257
ACS Omega 2024, 9, 18643−18653

PROGENy, indicating that inflammation-related signaling pathways, such as TNF-α, JAK-STAT, and NF-κB pathways scored higher in the IU and VKH groups. Of note, the Wnt pathway got the highest score in the IU group.

3.3. Identification of Key Subnetworks and Hub Proteins. PPI networks were generated and used to identify highly interconnected clusters (dense regions) of DEPs, which were defined as key subnetworks. Within these key subnetworks, the most highly correlated DEPs were defined as hub proteins. Figure 4A−C shows the key subnetworks of DEPs obtained from any two comparisons among VKH, IU, and the control group, with hub proteins represented as larger nodes. GO analysis of the proteins within the key subnetworks revealed that "complement and coagulation cascades" were the main enriched biological process in VKH and IU groups (Figure 4A,B), which highlights the pivotal role of complement reactions within the AH of uveitis. Enrichment analysis revealed that the key subnetworks of DEPs of the VKH and control groups were involved in "inflammatory response," "lysosome," "secretion by cell", and "cholesterol metabolic process" (Figure 4A). The key subnetworks of DEPs of the IU and control groups were "proteasome," "secretion by cell," "cholesterol metabolic process," "actin cytoskeleton organization," "lysosome," "complement activation of the classical pathway", and "negative regulation of Wnt signaling pathway" (Figure 4B). The key subnetworks of DEPs of the VKH and IU groups were enriched exclusively in "complement and coagulation cascades" (Figure 4C).

3.4. Biomarker Screening Using the XGBoost Algorithm. Machine learning algorithms were used to identify potential diagnostic biomarkers from 557 quantifiable proteins for distinguishing three groups of 44 samples. XGBoost is an integrated learning method that builds a strong ensemble classifier by combining multiple weak learners. Most importantly, XGBoost can improve the performance of the model by increasing the number of weak learners, and its regularization function can prevent overfitting. Since the number of features was much larger than that of samples, XGBoost was more suitable for this data set. Forty-four samples were divided into a training set and testing set to establish and validate a classification model, with the aim of screening important proteins from the 557 quantifiable proteins. To improve robustness, a final XGBoost classification model was determined after fivefold cross-validation and parameter optimization (e.g., learning rate and max-depth).

However, a total of 23 proteins were included in the model and ranked according to their relative importance (Figure 5A). In this model, the classification accuracy of the testing set reached 85.71%; other statistics regarding the confusion matrix are listed in Table 1. The κ index was used to assess the classification accuracy of the matrix and reached 0.7795, indicating substantial agreement. The per-class performance of this model applied to the testing set is shown in the confusion matrix in Figure 5B. ROC curves for the two-class and multiclass analyses are presented in Figure 5C, with the area under the curve (AUC) reaching 0.9333 for multiclass analyses. We observed that the top three ranked proteins were TF, complement factor B (CFB), and lysozyme C (LYZ), which achieved a summed importance score of >67%. Box plots of their expression values in VKH, IU, and controls revealed significant differences between the groups (Figure S3A). To improve clinical applicability, i.e., to achieve more efficient diagnostic performance with a minimum number of biomarkers, we subsequently validated the three most important proteins.

Table 1. Statistics of the Confusion Matrix in the Testing Set[a]

overall statistics		statistics by three class			
			control	VKH	IU
accuracy	85.71%	sensitivity	1.0000	0.6000	1.0000
95% CI	(0.5719, 0.9822)	specificity	0.8750	1.0000	0.9091
p-value	0.00128	PPV	0.8571	1.0000	0.7500
κ	0.7795	NPV	1.0000	0.8182	1.0000
		balanced accuracy	0.9375	0.8000	0.9545

[a]Abbreviation: CI, confidence interval; PPV, positive predictive value; NPV, negative predictive value.

3.5. Constructing a Decision Tree for Diagnostic Classification. To confirm the reliability of the three identified biomarker candidates, 24 AH samples from an independent validation cohort were included for validation using HR-MRM analysis. HR-MRM is a targeted proteomics technique typically performed by using high-resolution mass spectrometry. As shown in Figure S3B, the trends of TF, CFB, and LYZ expression from HR-MRM analysis (Table S4) were almost consistent with those in SWATH acquisition. TF and CFB exhibited the highest expression in the IU group, while LYZ expression was higher in the VKH group than in the IU group.

We subsequently constructed a simple classification decision tree using the quantitative values of the three proteins in the HR-MRM assays. Figure S3C shows the cp plot for the "rpart" fit to visualize the cross-validation results. As an appropriate cp for pruning is often the leftmost value for which the mean lies below the horizontal line, the cp value was set as 0.08. Eventually, TF and CFB were chosen for constructing this classification decision tree, and the thresholds were labeled (Figure 5D). The accuracies for the training and test sets are 93.75 and 87.50%, respectively.

4. DISCUSSION

Uveitis is a blinding eye disease affecting people worldwide, with IU and VKH as two common types of uveitis that have unknown etiology and require available markers for laboratory diagnosis. In the current study, we demonstrated that innate immune responses, in particular the complement cascade, exert important effects in the AH of patients with IU and VKH. Proteomic profiles of IU and VKH samples showed several pathological alterations including extracellular matrix (ECM) disruption, blood−AH barrier breakdown, and retinal cell damage, among others. Moreover, potential biomarker candidates were identified using XGBoost, and a classification decision tree consisting of TF and CFB was constructed after HR-MRM validation.

AH is a plasma-derived fluid and therefore contains the same components as plasma, albeit in significantly different relative amounts. Specifically, AH has more sodium ions, the principal ion that maintains osmotic pressure; more ascorbic acid and lactate; and less protein, only 1/200th of that in plasma.[13] The main AH component is ALB, followed by TF, IgA, and IgG.[14] Concordantly, we found that ALB and TF were the most abundant components in VKH, IU, and control groups. We also noted significantly higher ALB and TF levels in the VKH

https://doi.org/10.1021/acsomega.3c10257
ACS Omega 2024, 9, 18643−18653

and IU groups than in the control group, which may be attributed to the breakdown of the blood−AH barrier during inflammation, causing leakage of plasma ALB and TF into the AH. PTGDS is the most highly expressed gene in ciliary body tissue;[15] notably, PTGDS ranked second in AH protein abundance of the control group but was downregulated in both the VKH and IU groups, possibly owing to anterior chamber inflammation and ciliary body tissue injury. AH provides a homeostatic environment for the anterior chamber tissue and therefore contains various enzymes and enzyme-related proteins such as the Serpin family. Due to their relatively low abundances, MS detection of growth factors, cytokines, and receptors can be poor.[16] Consistently, interleukin (IL)-6, IL-1 receptor accessory protein (IL1RAP), and IL-18-binding protein (IL18BP) ranked last in protein abundance in this study. Poor MS detection of low-abundance proteins may also explain the low ranking of proteasome subunits, such as proteasome activator complex subunit 2 (PSME2), proteasome subunit α type-6 (PSMA6), and proteasome subunit α type-5 (PSMA5).

Volcano plots of comparisons between the two groups revealed several downregulated proteins common to the VKH and IU groups. Subsequent enrichment analysis indicated that these proteins had functions related to cell−cell adhesion and eye morphogenesis, which may explain the cellular inflammation and subsequent ocular tissue damage seen in IU and VKH. The most downregulated proteins could be grouped into two categories. One category included proteins associated with extracellular matrix organization, such as PTGDS, nesh-binding protein (ABI3BP), testican-1 (SPOCK1), FSTL1, and α-II spectrin (SPTAN1), and the downregulation of these proteins may account for inflammation-induced tissue destruction. The second category included proteins related to single-cell-type expression clusters localized to retinal cells, such as CLSTN1, RBP3, and carboxypeptidase E (CPE), which are relevant to retinal photoreceptor cells, neuroserpin (SERPINI1) and amyloid-like protein 2 (APLP2), which are relevant to bipolar cells, and wnt inhibitory factor 1 (WIF1), which is relevant to Muller cells (https://www.proteinatlas.org/).[17] AH is involved in the nutrient delivery and removal of metabolic products from the avascular tissues in the eye.[18] Several studies have already indicated that changes in AH protein levels were found in posterior segment disorders.[6,7] In addition, a recent study identified specific intracellular proteins from retinal cells in AH.[9] Therefore, our results highlighted the potential application of AH proteomic analysis in investigating ocular disease biology including that of fundus diseases.

Moreover, transforming growth factor β-1 (TGF-β1) and IL-6 were more highly expressed in the IU and VKH groups than in the control group, which is consistent with that of a previous study of experimental autoimmune uveitis (EAU).[19] TGF-β1, a multifunctional cytokine, plays a vital role in regulating cell proliferation, differentiation, and ECM neogenesis. It is mainly present in plasma but may leak into the AH following disruption of the blood−AH barrier. IL-6 is a pleiotropic cytokine involved in multiple activities that promote cell proliferation and differentiation, as well as accelerated APPs synthesis in hepatocytes. Ohta et al.[19,20] reported that at the onset of EAU induction, IL-6 dominates the immune response by antagonizing TGF-β, resulting in the loss of the immune-privileged state of AH. In contrast, in progressively severe EAU, IL-6 is absent, and high expression of plasma-derived TGF-β1 and ocular-derived TGF-β2 suppressed the progression of inflammation. Therefore, the IL-6/TGF-β balance appears to be a key determinant of AH inflammatory status and, consequently, uveitis initiation and progression. Our findings indicated that the AH proteome in patients with VKH and IU exhibits continued high expression of APPs despite the quiescence of intraocular inflammation, which may also be attributed to IL-6/TGF-β imbalance. A previous study reported that intraperitoneal injection of TGF-β1 can inhibit the progression of endotoxin-induced uveitis.[21] Similarly, increasing TGF-β levels and reducing IL-6 levels in AH may be promising therapeutic strategies to treat uveitis. Interleukin-18-binding protein (IL18BP) suppresses the downstream signal transduction of IL-18 by competitively binding to IL-18. Downregulation of IL18BP in the VKH and IU groups may therefore lead to increased levels of IL-18-induced IFN-γ production and Th1-type immune responses, which could then lead to uveitis development.

Enrichment analysis results demonstrated the critical role of the antimicrobial immune response, innate immune response, and complement cascade in AH. Despite the antimicrobial immune response, the importance of complement and coagulation cascades in the key subnetworks of DEPs led us to hypothesize that innate immune responses predominate in the AH environment. Despite many similar alterations in the biological processes in the AH of the two uveitis groups, there are still some significant differences. Of note, proteins within the "inflammatory response" subnetworks of the comparison between the VKH and control groups were related to innate immune cells. These proteins included CD16a antigen (FCGR3A), which triggers natural killer cells to destroy target tissues and enhance macrophage-mediated phagocytosis;[22] CD163 and v-set and immunoglobulin domain-containing protein 4 (VSIG4), which are markers of macrophage activation; CD14, which is a monocyte marker;[23−25] and Chitinase-3-like protein 1 (CHI3L1), which is expressed and secreted by various types of cells, including macrophages.[26]

Notably, negative regulation of the Wnt pathway was found in the key subnetworks of the comparison between the IU and control groups, with downregulation of the Wnt pathway inhibitors WIF1, dickkopf-related protein 3 (DKK3), and secreted frizzled-related protein 3 (FRZB) in AH suggesting an activated state of the Wnt pathway. Sugali et al.[27] reported that canonical Wnt signaling activators can prevent the adverse effects of glucocorticoids (GCs) in the eye. Specifically, the authors reported that DKK1, a Wnt pathway inhibitor, is elevated in the AH and trabecular meshwork (TM) of patients with glaucoma and enhanced glucocorticoid receptor (GR) signaling, indicating that GR and Wnt signaling are mutually inhibited in the TM. Moreover, the absence of endothelial GR accelerates diabetic renal fibrosis, partly through the upregulation of Wnt signaling.[28] We therefore suggest that the downregulation of Wnt signaling inhibitors in the AH of patients with IU leads to Wnt signaling activation and downregulation of GR signaling, thus leading to GC resistance and insensitivity to topical treatment. Accordingly, complementary treatment with Wnt pathway agonists may be an effective strategy for improving the efficacy of topical GC treatment.

In recent years, machine learning techniques have been implemented in disease prediction, classification, and diagnosis. The XGBoost algorithm, first released in 2016, is more complex than traditional machine learning algorithms,[29] and exhibits excellent performance over other machine learning

https://doi.org/10.1021/acsomega.3c10257
ACS Omega 2024, 9, 18643−18653

algorithms,[30,31] preventing overfitting by using the "feature subsampling" technique and providing efficient and flexible handling of missing data, as well as allowing faster work through parallel processing. In this study, a robust model based on an XGBoost-interpretable machine learning algorithm was built to screen potential biomarker candidates from the AH proteome. The expression levels of the top three identified proteins were validated by HR-MRM. HR-MRM is a high-throughput method for protein quantification and, therefore, is suitable for AH research. In the validation cohort, TF and CFB expressions were centrally distributed within groups, with nearly 2-fold intergroup differences. Therefore, the decision tree consisting of TF and CFB achieved good performance in VKH, IU, and control classification, indicating the substantial potential of this biomarker panel for future clinical application in uveitis diagnosis. However, large-scale sample validation is required. Furthermore, compared with traditional immunoassays, we highlighted the superiority of MS-based targeted protein quantification for the accurate detection of small-volume samples. To achieve this, the HR-MRM method with isotope-labeled peptides as internal references to generate accurate absolute quantitative values for determining the thresholds of the classification tree is required.[32]

There were some limitations in this study. Owing to ethical constraints, the current proteomics profiles cannot fully represent the characteristics of the disease, as all samples were obtained during the inactive inflammatory phase. In addition, the number of samples used in the machine learning pipeline was relatively small because of the slow collection of AH samples. Although the model was cross-validated, errors remained as a result of the small sample size. Therefore, multistage samples as well as larger sample sizes are necessary to obtain more robust results.

5. CONCLUSIONS

In conclusion, AH from patients with IU and VKH in the quiescent phase retained numerous highly expressed inflammation-associated proteins, resulting in a chronic state of low-level inflammation and rendering the patient prone to flare-ups. We identified ECM-related and retinal-cell-derived proteins in the AH, which deserve further investigation. In addition, the innate immune response was considered dominant in the AH of patients with VKH and IU, and the IL-6/TGF-β balance may be the key driver of disease development. Wnt signaling, as indicated by the AH of patients with IU, is also a promising treatment target. In addition, TF and CFB were identified and validated as promising biomarker panels for distinguishing VKH, IU, and control groups.

■ ASSOCIATED CONTENT

Data Availability Statement

All mass spectrometry proteomics data have been deposited to the ProteomeXchange Consortium via the PRIDE partner repository with the data set identifier PXD041318 and PXD043575. Data will be made available on request.

Supporting Information

The Supporting Information is available free of charge at https://pubs.acs.org/doi/10.1021/acsomega.3c10257.

Quality control (Figure S1); enrichment analysis of overlapping differentially expressed proteins, related to Figure 2 (Figure S2); expression levels of biomarker candidates and parameters of the decision tree, related to Figure 5 (Figure S3); demographic parameters of subjects included in the discovery and validation cohort (Table S1); normalized and log 2-transformed protein expression data from SWATH-MS (Table S2); results of differential expression analysis between the VKH, IU, and control group (Table S3); and normalized and log 2-transformed protein expression data from HR-MRM (Table S4) (PDF)

■ AUTHOR INFORMATION

Corresponding Author

Xiaomin Zhang − *Tianjin Key Laboratory of Retinal Functions and Diseases, Tianjin Branch of National Clinical Research Center for Ocular Disease, Eye Institute and School of Optometry, Tianjin Medical University Eye Hospital, Tianjin 300384, China;* orcid.org/0000-0003-4898-4152; Email: xzhang08@tmu.edu.cn

Authors

Lingzi Wu − *Tianjin Key Laboratory of Retinal Functions and Diseases, Tianjin Branch of National Clinical Research Center for Ocular Disease, Eye Institute and School of Optometry, Tianjin Medical University Eye Hospital, Tianjin 300384, China; Beijing Institute of Ophthalmology, Beijing Tongren Eye Center, Beijing Tongren Hospital, Capital Medical University, Beijing 100051, China*

Jinying An − *Tianjin Key Laboratory of Retinal Functions and Diseases, Tianjin Branch of National Clinical Research Center for Ocular Disease, Eye Institute and School of Optometry, Tianjin Medical University Eye Hospital, Tianjin 300384, China*

Xueru Li − *Tianjin Key Laboratory of Retinal Functions and Diseases, Tianjin Branch of National Clinical Research Center for Ocular Disease, Eye Institute and School of Optometry, Tianjin Medical University Eye Hospital, Tianjin 300384, China*

Qingqin Tao − *Tianjin Key Laboratory of Retinal Functions and Diseases, Tianjin Branch of National Clinical Research Center for Ocular Disease, Eye Institute and School of Optometry, Tianjin Medical University Eye Hospital, Tianjin 300384, China*

Zheng Liu − *Shanxi Eye Hospital, Taiyuan 030002 Shanxi, China*

Kai Zhang − *The Province and Ministry Co-sponsored Collaborative Innovation Center for Medical Epigenetics, Key Laboratory of Immune Microenvironment and Disease (Ministry of Education), Tianjin Key Laboratory of Medical Epigenetics, Department of Biochemistry and Molecular Biology, School of Basic Medical Sciences, Tianjin Medical University, Tianjin 300070, China*

Lei Zhou − *School of Optometry, Department of Applied Biology and Chemical Technology, and Research Centre for SHARP Vision (RCSV), The Hong Kong Polytechnic University, Hong Kong 999077, China; Centre for Eye and Vision Research (CEVR), Hong Kong 999077, China*

Complete contact information is available at: https://pubs.acs.org/10.1021/acsomega.3c10257

Author Contributions

[▽]L.W., J.A., and X.L. contributed equally to this work. Conceptualization: X.Z., L.Z., and K.Z.; data curation: L.W.,

https://doi.org/10.1021/acsomega.3c10257
ACS Omega 2024, 9, 18643−18653

J.A., X.L., Q.T., and Z.L.; formal analysis: L.W., J.A., and X.L.; funding acquisition: X.Z.; investigation: L.W., J.A., and X.L.; methodology: L.W., J.A., and X.L.; project administration: L.W., J.A., X.L., and Q.T.; supervision: X.Z., L.Z., and K.Z.; validation: L.W., J.A., and X.L.; visualization: L.W.; writing—original draft: L.W., J.A., X.L., and Q.T.; writing—review and editing: all authors. All authors read and approved the final manuscript.

Funding

This work was supported by the National Natural Science Foundation of China under grants 82171042 and 82371044; Tianjin Key Medical Discipline (Specialty) Construction Project under Grant TJYXZDXK-037A; Tianjin Medical University "Clinical Talent Training 123 Climbing Plan"; and Tianjin Binhai New Area Health Commission Science and Technology Project under Grant 2023BWKQ018.

Notes

The authors declare no competing financial interest.

■ ACKNOWLEDGMENTS

The authors are thankful to the Tianjin Medical University Eye Hospital Biobank for providing the biological samples used in this study.

■ REFERENCES

(1) Miserocchi, E.; Fogliato, G.; Modorati, G.; et al. Review on the worldwide epidemiology of uveitis. *Eur. J. Ophthalmol.* **2013**, *23* (5), 705−717.

(2) Deschenes, J.; Murray, P. I.; Rao, N. A.; et al. International Uveitis Study Group (IUSG): Clinical classification of uveitis. *Ocul. Immunol. Inflammation* **2008**, *16* (1), 1−2.

(3) Han, Y. S.; Rivera-Grana, E.; Salek, S.; et al. Distinguishing uveitis secondary to sarcoidosis from idiopathic disease: Cardiac implications. *JAMA Ophthalmol.* **2018**, *136* (2), 109−115.

(4) Yang, P.; Zhang, Z.; Zhou, H.; et al. Clinical patterns and characteristics of uveitis in a tertiary center for uveitis in China. *Curr. Eye Res.* **2005**, *30* (11), 943−948.

(5) Du, L.; Kijlstra, A.; Yang, P. Vogt−Koyanagi−Harada disease: Novel insights into pathophysiology, diagnosis and treatment. *Prog. Retinal Eye Res.* **2016**, *52*, 84−111.

(6) Rinsky, B.; Beykin, G.; Grunin, M.; et al. Analysis of the aqueous humor proteome in patients with age-related macular degeneration. *Invest. Ophthalmol. Visual Sci.* **2021**, *62* (10), 18.

(7) Ma, Z.; Liu, J.; Li, J.; et al. Klotho levels are decreased and associated with enhanced oxidative stress and inflammation in the aqueous humor in patients with exudative age-related macular degeneration. *Ocul. Immunol. Inflammation* **2022**, *30* (3), 630−637.

(8) Smith, D. W.; Lee, C. J.; Gardiner, B. S. No flow through the vitreous humor: How strong is the evidence? *Prog. Retinal Eye Res.* **2020**, *78*, No. 100845, DOI: 10.1016/j.preteyeres.2020.100845.

(9) Wolf, J.; Rasmussen, D. K.; Sun, Y. J.; et al. Liquid-biopsy proteomics combined with AI identifies cellular drivers of eye aging and disease in vivo. *Cell* **2023**, *186* (22), 4868.e12−4884.e12.

(10) Wu, J. X.; Song, X.; Pascovici, D.; et al. SWATH Mass Spectrometry Performance Using Extended Peptide MS/MS Assay Libraries. *Mol. Cell. Proteomics* **2016**, *15* (7), 2501−2514.

(11) Zhou, Y.; Zhou, B.; Pache, L.; et al. Metascape provides a biologist-oriented resource for the analysis of systems-level datasets. *Nat. Commun.* **2019**, *10* (1), No. 1523.

(12) Schubert, M.; Klinger, B.; Klünemann, M.; et al. Perturbation-response genes reveal signaling footprints in cancer gene expression. *Nat. Commun.* **2018**, *9* (1), No. 20.

(13) Coté, G. L.; Cameron, B. D. A Noninvasive Glucose Sensor Based on Polarimetric Measurements Through the Aqueous Humor of the Eye. In *Handbook of Optical Sensing of Glucose in Biological Fluids and Tissues*; Tuchin, V. V., Ed.; CRC Press Inc., 2009; pp 183−211.

(14) Bours, J. The protein distribution of bovine, human and rabbit aqueous humour and the difference in composition before and after disruption of the blood/aqueous humour barrier. *Lens Eye Toxic. Res.* **1990**, *7* (3−4), 491−503.

(15) Carnes, M. U.; Allingham, R. R.; Ashley-Koch, A.; et al. Transcriptome analysis of adult and fetal trabecular meshwork, cornea, and ciliary body tissues by RNA sequencing. *Exp. Eye. Res.* **2018**, *167*, 91−99.

(16) Chowdhury, U. R.; Madden, B. J.; Charlesworth, M. C.; et al. Proteome analysis of human aqueous humor. *Invest. Ophthalmol. Visual Sci.* **2010**, *51* (10), 4921−4931.

(17) Thul, P. J.; et al. A subcellular map of the human proteome. *Science* **2017**, *356* (6340), No. eaal3321, DOI: 10.1126/science.aal3321.

(18) Ji, Y.; Rao, J.; Rong, X.; et al. Metabolic characterization of human aqueous humor in relation to high myopia. *Exp. Eye Res.* **2017**, *159*, 147−155.

(19) Ohta, K.; Wiggert, B.; Yamagami, S.; et al. Analysis of immunomodulatory activities of aqueous humor from eyes of mice with experimental autoimmune uveitis. *J. Immunol.* **2000**, *164* (3), 1185−1192.

(20) Ohta, K.; Yamagami, S.; Taylor, A.; et al. IL-6 antagonizes TGF-beta and abolishes immune privilege in eyes with endotoxin-induced uveitis. *Invest. Ophthalmol. Visual Sci.* **2000**, *41* (9), 2591−2599.

(21) Peng, B.; Li, Q.; Roberge, F.; et al. Effect of transforming growth factor beta-1 in endotoxin-induced uveitis. *Invest. Ophthalmol. Visual Sci.* **1997**, *38* (1), 257−260.

(22) Kremer, P. G.; Barb, A. W. The weaker-binding Fc γ receptor IIIa F158 allotype retains sensitivity to N-glycan composition and exhibits a destabilized antibody-binding interface. *J. Biol. Chem.* **2022**, *298* (9), No. 102329.

(23) Yap, Y. J.; Wong, P. F.; AbuBakar, S.; et al. The clinical utility of CD163 in viral diseases. *Clin. Chim. Acta* **2023**, *541*, No. 117243.

(24) Liu, B.; Cheng, L.; Gao, H.; et al. The biology of VSIG4: Implications for the treatment of immune-mediated inflammatory diseases and cancer. *Cancer Lett.* **2023**, *553*, No. 215996.

(25) Wu, Z.; Zhang, Z.; Lei, Z.; et al. CD14: Biology and role in the pathogenesis of disease. *Cytokine Growth Factor Rev.* **2019**, *48*, 24−31.

(26) Tizaoui, K.; Yang, J. W.; Lee, K. H.; et al. The role of YKL-40 in the pathogenesis of autoimmune diseases: a comprehensive review. *Int. J. Biol. Sci.* **2022**, *18* (9), 3731−3746.

(27) Sugali, C. K.; Rayana, N. P.; Dai, J.; et al. The canonical wnt signaling pathway inhibits the glucocorticoid receptor signaling pathway in the trabecular meshwork. *Am. J. Pathol.* **2021**, *191* (6), 1020−1035.

(28) Srivastava, S. P.; Zhou, H.; Setia, O.; et al. Loss of endothelial glucocorticoid receptor accelerates diabetic nephropathy. *Nat. Commun.* **2021**, *12* (1), No. 2368.

(29) Chen, T.; Guestrin, C.et al. In *XGBoost: A Scalable Tree Boosting System*, Proceedings of the 22nd ACM Sigkdd International Conference on Knowledge Discovery and Data Mining, San Francisco, 2016; pp 785−794.

(30) Shah, A. A.; Devana, S. K.; Lee, C.; et al. Prediction of major complications and readmission after lumbar spinal fusion: A machine learning-driven approach. *World Neurosurg.* **2021**, *152*, e227−e234.

(31) Yang, P.; Wu, T.; Yu, M.; et al. A new method for identifying the acute respiratory distress syndrome disease based on noninvasive physiological parameters. *PLoS One* **2020**, *15* (2), No. e0226962.

(32) Tong, L.; Zhou, X. Y.; Jylha, A.; et al. Quantitation of 47 human tear proteins using high resolution multiple reaction monitoring (HR-MRM) based-mass spectrometry. *J. Proteomics* **2015**, *115*, 36−48.

https://doi.org/10.1021/acsomega.3c10257
ACS Omega 2024, 9, 18643−18653